International Journal of Thermal Sciences 120 (2017) 469–480

Contents lists available at ScienceDirect

International Journal of Thermal Sciences

journal homepage: www.elsevier.com/locate/ijts

Theoretical, numerical, and experimental investigation of pressure rise due to deflagration in confined spaces

Boo-Hyoung Bang [a, b, 1], Chan-Sol Ahn [a, c, 1], Jong-Gun Lee [a], Young-Tae Kim [b], Myung-Ho Lee [b], Brad Horn [d], Darren Malik [d], Kelly Thomas [d], Scott C. James [e], Alexander L. Yarin [f, *], Sam S. Yoon [a, **]

[a] School of Mechanical Engineering, Korea University, Seoul, 136-713, South Korea
[b] Technology Development Team, Daewoo Inst. of Const. Tech., 60, Songjuk-dong, Jangan-gu, 440-210, Suwon, South Korea
[c] Fire Research Center, Korea Institute of Construction Technology, 283, Goyang-daero, Ilsanseo-gu, 10223, Goyang-si, South Korea
[d] Baker Engineering and Risk Consultants, INC, 3330 Oakwell Court, Suite 100, San Antonio, TX 78218, USA
[e] Depts. of Geosciences and Mech. Eng., Baylor University, Waco, TX 76798, USA
[f] Department of Mechanical & Industrial Engineering, University of Illinois at Chicago, 842 W. Taylor St., Chicago 60607, USA

ARTICLE INFO

Article history:
Received 31 January 2017
Received in revised form
19 May 2017
Accepted 19 May 2017
Available online 7 June 2017

ABSTRACT

Estimating pressure rise due to deflagration in a fully or partially confined space is of practical importance in safety design of a petrochemical plant. Herein, we have developed a new theoretical model to predict the pressure rise due to deflagration in both fully and partially confined spaces. First, the theoretical model was compared and validated against experimental data from the closed-space experiments with hydrogen, methane, propane, and ethane. The theory predicted accurate pressure rises near the stoichiometric regime for all fuel types; outside the stoichiometric regime, especially, for rich mixtures of hydrocarbons with air, the theory over-predicted pressure rise since it does not account for soot formation and the associated energy losses by radiation. Experimental investigation of propane and hydrogen deflagration was conducted in a partially confined space and the theory-based predictions agreed with the data up to 5%. Parametric numerical study was performed to investigate the effect of the initial pressure and temperature of gaseous fuels on pressure rise.

1. Introduction

Safety of petrochemical plants is a primary consideration in their design. Although explosions at petrochemical plants are rare, they can happen due to fuel leakage from outdated or malfunctioning devices. Typically, leaks are detected early and disaster is thus mitigated. However, when detection system fails or the plant is subject to an unexpected situation (e.g., a terrorist attack), fuel leaks can be considerable and could lead to catastrophic explosions. To minimize damage from potential explosions, safety factors must be incorporated into the structural designs for pipes and storage tanks. Because mostly structural damage is inflicted by a sudden increase in pressure due to an explosion, accurate predictions of pressure rise are required.

Explosions are categorized as either detonations or deflagrations depending on the flame propagation speed. When the flame speed is supersonic, it is associated with *detonation* wave which incorporate a shock wave as in some bomb explosions. On the other hand, *deflagration* is characterized by a low subsonic flame speed and is characteristic of gas explosions studied here in relation to hydrogen, methane, propane, and ethane explosions. Fuel gas leakage and ignition may occur inside a confined space where the pressure increase could be sufficient to rupture the confining structure. A liquid fuel tank located close to a fire experiences heating and its content may boil, leading to highly pressurized fuel tank that eventually ruptures resulting in an explosion of the boiling-liquid and expanding-vapor. Even in an open space, a pressure rise can happen due to obstacles. For this reason, we considered deflagration in both confined and partially-confined systems.

Jo and Crowl [1,2] proposed a flame-growth model to predict the maximum pressure from hydrogen and methane explosions in a

* Corresponding author.
** Corresponding author.
E-mail addresses: ayarin@uic.edu (A.L. Yarin), skyoon@korea.ac.kr (S.S. Yoon).
[1] Equal contribution.

http://dx.doi.org/10.1016/j.ijthermalsci.2017.05.019
1290-0729/

confined vessel. Zhou et al. [3] compared their model against experimental data for a premixed laminar flame case. Razus et al. [4] experimentally investigated pressure rise resulting from propane explosion in a confined space at different initial pressure and temperature. Mitu et al. [5] acquired data on pressure rise due to ethane explosion in a confined space for the initial pressure (P_0) and temperature (T_0) ranges of 20–130 kPa and 298–423 K, respectively. Bang et al. [6,7] predicted pressure rise resulting from a worst-case scenario of strong explosion of hydrogen in an open space. Luijten et al. [8] presented a laminar flame speed model to predict the maximum pressure rise in a confined area. For deflagration, the model proposed by Jo and Crowl [2] was shown to be more accurate than its competitors listed in that work. However, their model is sensitive to the specified flame speed for a given fuel concentration, which requires acquisition of the instance-specific data, and is hence impractical for situations with different fuel types and concentrations. A more versatile model that does not require flame-speed data is required.

To address this issue, here we propose a general and simple deflagration model which determines the flame speed. We demonstrate the accuracy of this model by comparing its predictions to the experimental data for hydrogen, methane, propane, and ethane combustion in a confined space. Moreover, we study experimentally deflagration of propane and hydrogen in a partially confined space, and use these data to further validate our model. Lastly, parametric numerical study aims at the effect of the initial pressure and temperature p_0 and T_0, respectively, on the overall pressure rise.

2. Theoretical and numerical models

2.1. Theoretical model for confined areas

Combustion can be accompanied by pressure rise [9]. The aim of the present sub-section is to evaluate and compare it with the experimental evidence.

The balance of the total (physical and chemical) internal energy E reads

$$E(T_0) = E(T_{bv}), \tag{1}$$

where T_0 is the initial temperature and T_{bv} is the temperature of combustion products.

Because

$$E(T_0) = c_{v,eq}T_0 + QC_f, \tag{2}$$

$$E(T_{bv}) = c_{v,eq}T_{bv}, \tag{3}$$

one obtains from Eqs. (1)–(3) that

$$T_{bv} = T_0 + \frac{Q}{c_{v,eq}}C_f, \tag{4}$$

where Q is the heat release per unit mass of reactive mixture and $c_{v,eq}$ is the equivalent specific heat of the fuel-air-products mixture at constant volume. C_f is the dimensionless initial fuel concentration in the reactive mixture (either lean, stoichiometric, or rich),

$$C_f = \frac{M_f}{M_f + M_{air}}. \tag{5}$$

The equivalent specific heat is evaluated as

$$c_{v,eq} = \frac{c_{v,f}M_f + c_{v,air}M_{air}}{\mu_{eq}\left(M_f/\mu_f + M_{air}/\mu_{air}\right)}. \tag{6}$$

In Eqs. (5) and (6), M_f and M_{air} are the initial masses of fuel and air in the mixture, respectively, $c_{v,f}$ and $c_{v,air}$ are the specific heats of the fuel and air, respectively, μ_f and μ_{air} are the molecular masses of the fuel and air, respectively, and μ_{eq} is the equivalent molecular weight of the fuel-air-products mixture.

Consider the situation when M_{air} is fixed, while M_f can vary. Then, according to Eq. (4) through (6) the combustion temperatures are given by the following expressions:

(i) For lean mixtures ($M_f < M_{f,s}$)

$$T_{bv} = T_0 + \frac{Q}{c_{v,eq}}\frac{M_f}{M_f + M_{air}}. \tag{7}$$

(ii) For a stoichiometric mixture ($M_f = M_{f,s}$)

$$T_{bv} = T_0 + \frac{Q}{c_{v,eq}}\frac{M_{f,s}}{M_{f,s} + M_{air}}. \tag{8}$$

(iii) For the rich mixtures ($M_f > M_{f,s}$)

$$T_{bv} = T_0 + \frac{Q}{c_{v,eq}}\frac{M_{f,s}}{M_f + M_{air}}, \tag{9}$$

with $M_{f,s}$ being the stoichiometric fuel mass.

The molar concentration of fuel $C_{f,\,molar}$, a parameter given in the experiments, is

$$C_{f,molar} = \frac{M_f/\mu_{fuel}}{M_f/\mu_{fuel} + M_{air}/\mu_{air}}. \tag{10}$$

Using Eq. (10), Eqs. (7)–(9) can be transformed into:

(i) For lean mixtures ($M_f < M_{f,s}$)

$$T_{bv} = T_0 + \frac{Q}{c_{v,eq}}\frac{C_{f,molar}}{C_{f,molar} + \left(\mu_{air}/\mu_{fuel}\right)\left(1 - C_{f,molar}\right)}. \tag{11}$$

(ii) For a stoichiometric mixture ($M_f = M_{f,s}$)

$$T_{bv} = T_0 + \frac{Q}{c_{v,eq}}\frac{C_{f,molar,s}}{C_{f,molar,s} + \left(\mu_{air}/\mu_{fuel}\right)\left(1 - C_{f,molar,s}\right)}. \tag{12}$$

(iii) For rich mixtures ($M_f > M_{f,s}$)

$$T_{bv} = T_0 + \frac{Q}{c_{v,eq}}\left(\frac{C_{f,molar,s}}{1 - C_{f,molar,s}}\right)\frac{1}{C_{f,molar}/\left(1 - C_{f,molar}\right) + \left(\mu_{air}/\mu_{fuel}\right)}. \tag{13}$$

For combustion, the internal energy balance requires that for a spatially averaged temperature, $\overline{T}$, and the spatially averaged fuel concentration, $\overline{C}_f$, the following equality holds

$$E(T_0) = E(\overline{T}), \tag{14}$$

which means that

$$\overline{T} = T_0 + \frac{Q}{c_{v,eq}}\left(C_f - \overline{C}_f\right). \tag{15}$$

Using Eqs. (4) and (15) yields

$$\frac{\overline{T} - T_0}{T_{bv} - T_0} = 1 - \frac{\overline{C}_f}{C_f} = \eta, \tag{16}$$

where η indicates the completeness of combustion.

The equation of state applied to the effective volume occupied by fuel, air, and combustion products, V_0, is

$$pV_0 = \frac{M}{\mu_{eq}} R\overline{T}, \tag{17}$$

where p is pressure.

Equations (15)–(17) relate pressure to the completeness of combustion

$$p = \frac{MR}{\mu_{eq} V_0}\left(T_0 + \frac{QC_f}{c_{v,eq}}\eta\right). \tag{18}$$

Equations (4) and (18) indicate that

$$p = p_0[1 + (\varepsilon - 1)\eta], \tag{19}$$

where p_0 is the initial pressure and $\varepsilon = T_{bv}/T_0 > 1$. In particular, the pressure achieved at the end of the combustion process (i.e. $\eta = 1$), p_{end}, is

$$\frac{p_{end}}{p_0} = \varepsilon, \tag{20}$$

with $\varepsilon = T_{bv}/T_0$ calculated from Eqs. (11)–(13).

2.2. Numerical model for partially-confined areas

The thermodynamic theory developed in sub-section 2.1 can be applied not only to a completely confined space, but also to a partially confined space by tuning the completeness of combustion (η); therefore, the model is versatile and useful for various explosion scenarios. Because the analytical model does not consider any heat losses (e.g. radiation losses due to soot formation), it has a tendency to over-predict pressure rise in rich hydrocarbon fuels, as is shown below. Therefore, the thermodynamic theory of sub-section 2.1 would be expected to be a useful conservative estimate for such cases. However, an over-estimated pressure rise could impact plant financing if construction costs are derived from an excessively conservative estimate. For this reason, more detailed simulations such as a fully three-dimensional model may be required.

Structures located away from a potential explosion are subjected to much lower pressures compared to the maximum pressure near the source. In addition, if there are many obstacles between the explosion and the structure of interest, then the structure would be subjected to a much lower pressure than the maximum pressure, commensurately reducing the required protection scheme. For this reason, a fully 3D computational fluid dynamics tool, FLACS [10], has been used to simulate 3D distributions of pressure and temperature for various explosion scenarios.

The governing equations used in FLACS include the mass (21), momentum (22), enthalpy (23), fuel (24), and turbulent kinetic energy balances (25) plus the equation for the dissipation rate of the turbulent kinetic energy (26)

$$\frac{\partial \rho}{\partial t}(\beta_v \rho) + \frac{\partial}{\partial x_j}\left(\beta_j \rho u_j\right) = \frac{\dot{m}}{V}, \tag{21}$$

$$\frac{\partial}{\partial t}(\beta_v \rho u_i) + \frac{\partial}{\partial x_j}\left(\beta_j \rho u_i u_j\right) = -\beta_v \frac{\partial P}{\partial x_i} + \frac{\partial}{\partial x_j}\left(\beta_j \sigma_{ij}\right) + F_{o,i} + \beta_v F_{w,i} + \beta_v(\rho - \rho_0) g_i, \tag{22}$$

$$\frac{\partial}{\partial t}(\beta_v \rho h) + \frac{\partial}{\partial x_j}\left(\beta_j \rho h u_j\right) = \frac{\partial}{\partial x_j}\left(\beta_j \frac{\mu_{eff}}{\sigma_h}\frac{\partial h}{\partial x_j}\right) + \beta_v \frac{DP}{Dt} + \frac{\dot{Q}}{V}, \tag{23}$$

$$\frac{\partial}{\partial t}\left(\beta_v \rho r_{fuel}\right) + \frac{\partial}{\partial x_j}\left(\beta_j \rho u_j k\right) = \frac{\partial}{\partial x_j}\left(\beta_j \frac{\mu_{eff}}{\sigma_{fuel}}\frac{\partial r_{fuel}}{\partial x_j}\right) + R_{fuel} \tag{24}$$

$$\frac{\partial}{\partial t}(\beta_v \rho k) + \frac{\partial}{\partial x_j}\left(\beta_j \rho u_j k\right) = \frac{\partial}{\partial x_j}\left(\beta_j \frac{\mu_{eff}}{\sigma_k}\frac{\partial k}{\partial x_j}\right) + \beta_v P_k - \beta_v \rho \varepsilon, \tag{25}$$

$$\frac{\partial}{\partial t}(\beta_v \rho \varepsilon) + \frac{\partial}{\partial x_j}\left(\beta_j \rho u_j \varepsilon\right) = \frac{\partial}{\partial x_j}\left(\beta_j \frac{\mu_{eff}}{\sigma_\varepsilon}\frac{\partial \varepsilon}{\partial x_j}\right) + \beta_v P_\varepsilon - C_{2\varepsilon}\beta_v \rho \frac{\varepsilon^2}{k}, \tag{26}$$

where $F_{o,i}$ is flow resistance due to sub-grid obstructions and $F_{w,i}$ is flow resistance due to walls. β_v is volume porosity, β_j is area porosity, ρ is the density of the gas mixture, x_i are the Cartesian coordinates, u_i are the velocity components, $\dot{m}$ is mass release rate, V is volume where the mass is released, g is gravity, P is pressure, and σ_{ij} is the stress tensor. $\dot{Q}$ is the rate of heat release in the combustion reaction, r_{fuel} is the fuel mass fraction and R_{fuel} is the fuel reaction rate.

Semi-empirical constants used in the k-ε turbulence model are taken from Launder et al. [11]. The compressible 3D Navier-Stokes equations are solved using the finite-volume method. FLACS uses a second-order scheme to resolve diffusive terms and a second-order hybrid scheme to resolve convective terms. The time marching steps are advanced by a first-order backward Euler scheme to ensure numerical stability. The Semi-Implicit Method for Pressure-Linked Equations (SIMPLE), the pressure-correction algorithm [12] is applied and modified to handle compressible flows with an extra source terms, which accounts for the work done by compression in the enthalpy equation. Iterations are repeated until a mass residual of less than 10^{-4} is obtained.

The influence of the wall is modeled using a wall function where the dimensionless wall distance is:

$$y^+ = \frac{\rho C_\mu^{0.25} k^{0.5} y}{\mu}, \tag{27}$$

where y is the distance from the wall point to the wall. The wall point is defined as the point closest to the wall where transport equations are solved. The wall friction term in the momentum equation becomes

$$F_{w,i} = -\beta_v \tau_{w,i} \frac{A_w}{V}, \tag{28}$$

Here A_w is the area of the wall and $\tau_{w,i}$ is the shear stresses caused by the wall given by

$$\tau_{w,i} = \begin{cases} \mu \dfrac{u_i}{y} & if \quad y^+ < E^+ \\ \dfrac{\rho u_i \kappa C_\mu^{0.25} k^{0.5}}{\kappa E^+ + \ln\left(\dfrac{y^+}{E^+}\right)} & if \quad y^+ \geq E^+ \end{cases}, \tag{29}$$

where E^+ is a constant in wall functions and κ is the von Karman constant.

Laminar burning velocity is a function of pressure

$$S_L = S_L^0 \left(\frac{P}{P_0}\right)^{\gamma_P}, \tag{30}$$

where γ_P is a fuel-dependent parameter. In the quasi-laminar regime, the turbulent burning velocity is:

$$S_{QL} = S_L \left\{ 1 + a \min\left[\left(\frac{R}{3}\right)^{0.5}, 1 \right] \right\}, \tag{31}$$

where R is the flame radius and a is a fuel-dependent constant.

The turbulent burning velocity is a simplified form of the expression [13]:

$$\frac{S_T}{S_L} = 0.875 K^{-0.392} \frac{u'}{S_L}, \tag{32}$$

where K is the Karlovitz stretch factor. The Courant-Friedrichs-Levy number based on fluid flow velocity is 0.5, which means that each time step is assigned so that fluid propagates only about half the length of a finite-volume cell each time step. The simulation duration was limited to 0.5 s, which is long enough for an exploding gas to achieve maximum pressure. Simulations were conducted on a 3.30-GHz PC with 8 cores × 2 processors and 128 GB of RAM. Fig. 2 shows the actual experimental space in which an explosive gas was contained. In FLACS, this container of 7.3 × 14.6 × 3.7 m^3 dimensions was included inside the computational domain of 100 × 100 × 50 m^3. The Euler equations are discretized for a boundary element. The stagnant air at an ambient temperature of 303 K was used as an initial condition. The computational geometry is depicted in Figs. 2–4. Inside the container, about 200 5-cm-diameter cylindrical stainless steel pipes were regularly aligned to simulate a congested-space scenario as shown in Fig. 3, which also indicates the steel walls as thick, black lines with the open side temporarily sealed with a plastic sheet (see Fig. 1).

2.3. Experiments for model validation

To validate numerical predictions from FLACS, the experimental apparatus in Fig. 2 was filled with an explosive gas. Total flammable volume is 391.5 m^3. The vertical pipes in Fig. 3 create congestion, induce turbulence to increase flame speed. As a result, the designed congestion due to the pipes produced a relatively high pressure, as opposed to the case without the pipes. The fuel-air mixture was ignited near the center of the rear wall to produce a vapor cloud explosion (VCE). The partially confined VCE could vent through the open side producing external blast loads and, in close proximity, fire exposure as the flame escaped the test apparatus and the expelled unburned gas continued to burn.

As shown in Fig. 4, multiple pressure gauges were installed at different locations on the floor, walls, columns, and roof. To identify asymmetries, pressure gauges were installed in pairs with

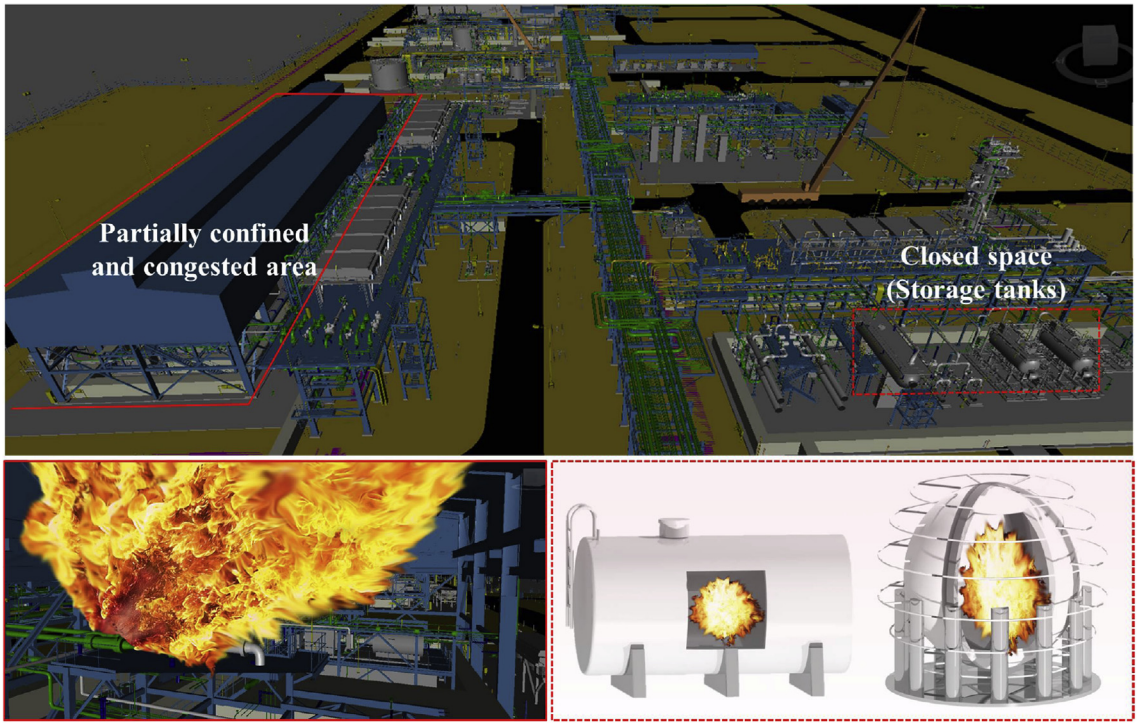

Fig. 1. Schematic of possible explosion scenarios in petrochemical plant. The bottom left shows an explosion in a congested area and the bottom right shows an explosion in a confined tank.

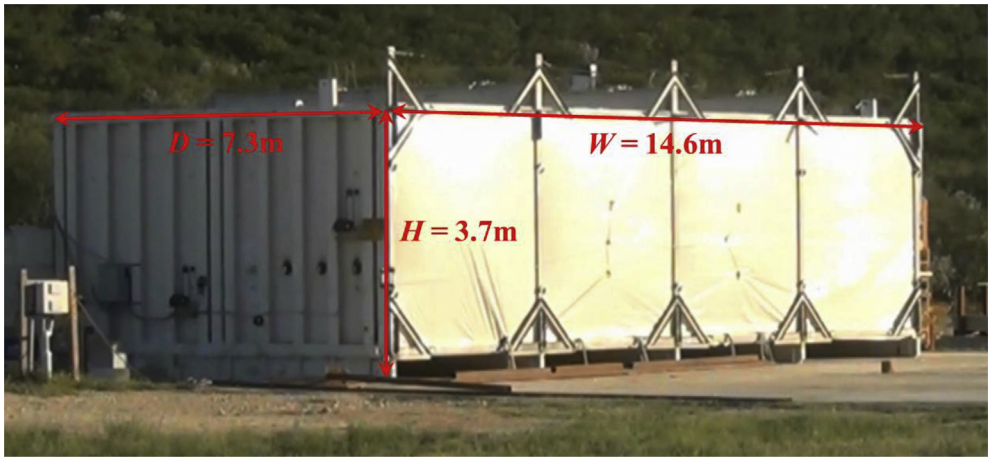

Fig. 2. Experimental setup for gas explosion.

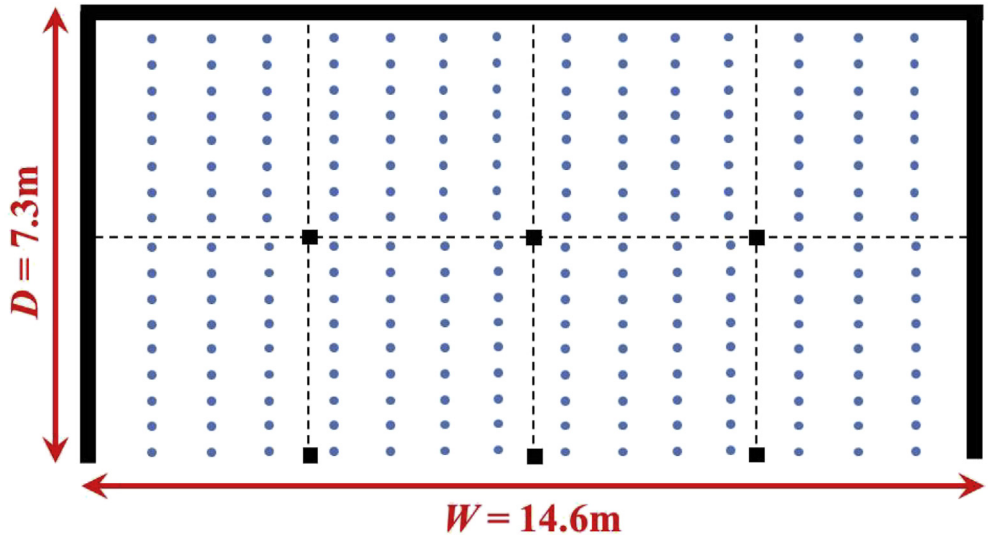

Fig. 3. Layout of the 5-cm-diameter cylinders to simulate a congested space.

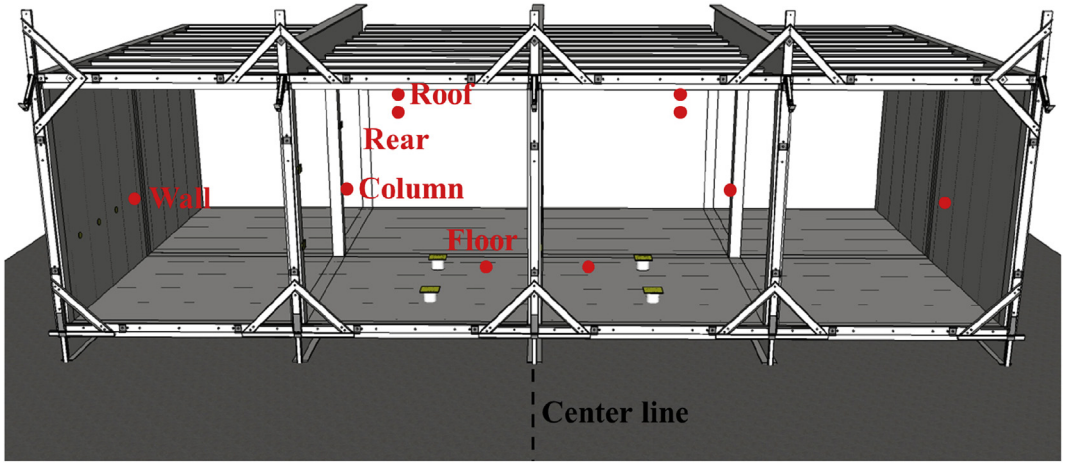

Fig. 4. Interior overpressure gauge locations.

Table 1
Case study for comparison of Eqs. (19) and (20) with experiments.

	Fuel	Oxidizer	Calculated range with *MF* [%]	Q (LHV) [MJ/kg]	Reference
Case 1	Hydrogen	Air	5–70	120	Sheroeder et al.
Case 2	Methane		4–16	50	Cashdollar et al.
Case 3	Propane		2–10	46	
Case 4	Ethane		3–10	47.8	Holtappels et al.

symmetric locations. Pressure, high-speed video (3000 fps), and high-definition video (30 fps) were recorded for all tests. A total of 17 dynamic pressure gauges captured the pressure history within and outside the experimental apparatus, with 10 and 7 pressure gauges for the interior and exterior locations, respectively. Because of the symmetrical locations of the interior gauges, only 5 sets of data are presented for Rear, Wall, Column, Floor, and Roof locations, as described in Fig. 4. Additional 7 pressure gauges were used for the exterior locations from MP1 to MP7. These exterior gauges were located at the center line, noted in Fig. 4, with at the distances of $z = 11.9, 16.5, 22.6, 30.2, 37.8, 45.4$, and 53 m away from the open end of the exploding container.

The pressure measurement system consisted of dynamic pressure gauges cabled to line-powered signal conditioners. Once the target fuel concentration was obtained, the fans used to circulate the fuel-air mixture were shut off for a period of 4 min prior to ignition to allow the mixture to become quiescent and eliminate any pre-ignition turbulence. Finally, the cloud was ignited with a low energy (~50 J) exploding fuse wire at the center of the back wall.

3. Results and discussion

3.1. Thermodynamic theory versus experiment data

The theoretically predicted pressures of the gas explosions were estimated using Eq. (19) for the different fuel types (hydrogen, methane, propane, and ethane) whose initial pressure (p_0) and temperature (T_0) varied depending on the scenario. In addition, the initial fuel mole fraction, *MF*, was also varied. Ultimately, the maximum pressure rise, p_{max}, was studied as a function of p_0, T_0, and *MF*.

Table 1 lists the four explosion scenarios considered. Because hydrogen and other hydrocarbon fuels have been widely used in petrochemical plants, p_{max} as a function of *MF* (or concentration) is of significant interest to petrochemical engineers. Air is the oxidizer for all explosions. Heat release in combustion is greatest for hydrogen (120 MJ/kg) while other fuels belong to the 45–50 MJ/kg range. *MF* for hydrogen was varied from 5 to 70% (30% stoichiometric). The *MF* for other fuels belonged to the 2–16% range (the stoichiometric values of 9.5, 4.5, and 6% for methane, propane, and

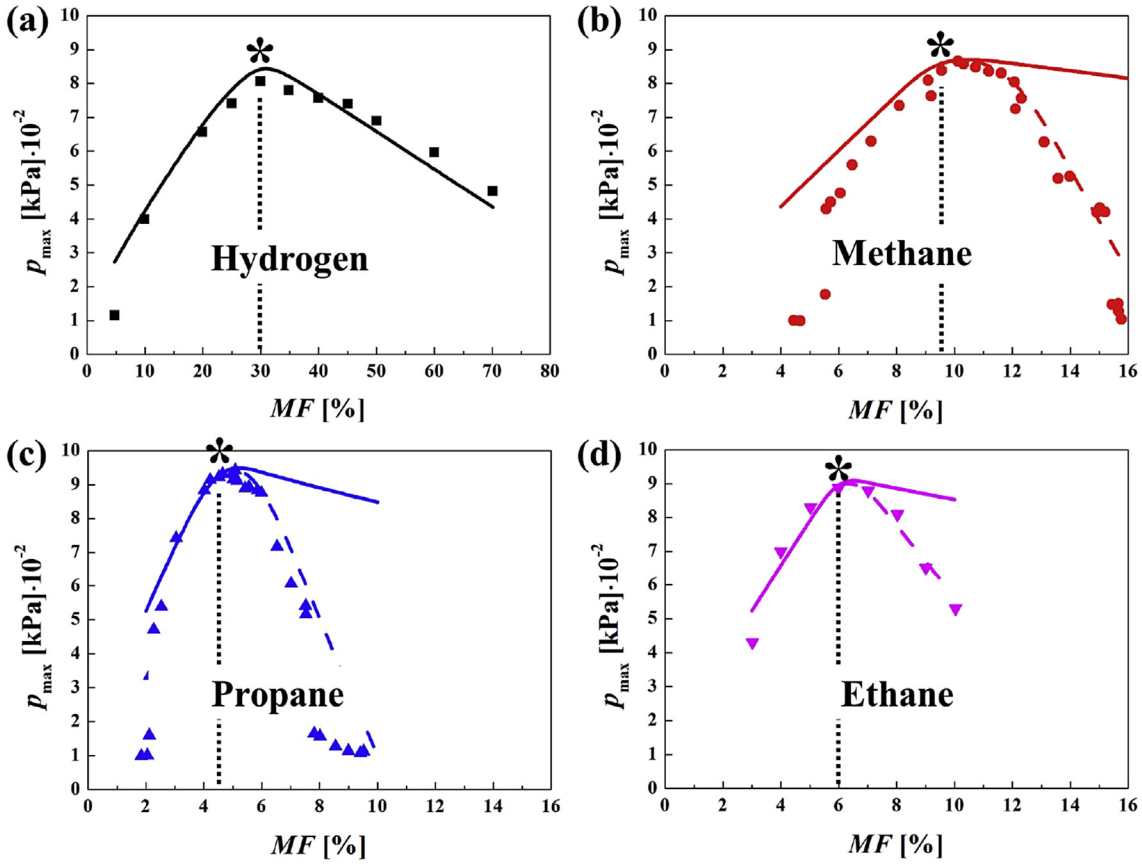

Fig. 5. Comparison of p_{max} predicted by the theory of sub-section 2.1, in particular, Eq. (19), for hydrogen experiments [14–16] at $T_0 = 298$ K and hydrocarbons experiments [14–16] at $T_0 = 293$ K. The stoichiometric MF is indicated with an asterisk.

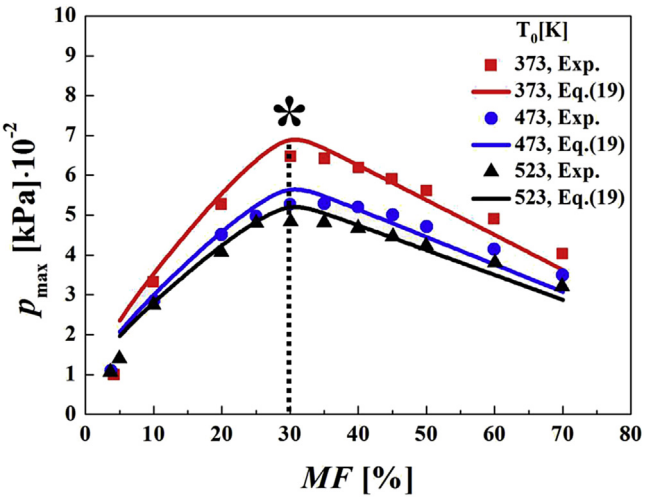

Fig. 6. Comparison of p_{max} from Eq. (19) with the data from the hydrogen experiments with different values of T_0.

ethane, respectively). All experiments in the previous studies [14–16] were acquired in a closed space suggesting a near complete combustion at the end, namely $\eta_e = 1$. They also imply no heat loss because of the closed space. The value of the completeness of combustion, η_e, should be considered as a fitting parameter depending on whether combustion takes place in an open, partially closed, or completely closed space because heat losses can vary significantly.

If the burning velocity is not fast enough, some of the unburned gas mixture is expelled from the partially closed confinement without being burned ($\eta_e < 1$) resulting in a lower final pressure. In other words, $\eta_e = 1$ implies a sufficiently high burning velocity when the entire fuel-oxidizer mixture is rapidly burned, even though the confinement can be partially open, i.e. this yields a conservative estimate of the highest possible pressure.

Fig. 5 compares p_{max} for hydrogen, methane, propane, and ethane deflagration. The solid curves are the theoretical predictions of subsection 2.1, in particular, Eq. (19) and the symbols are the experimental data from Refs. [14–16]. The dashed theoretical curves account for the radiation losses due to soot formation and are discussed below. For all cases, $8 < p_{max} < 10$ bar was observed for stoichiometric mixtures. In Fig. 5a the theoretical predictions for hydrogen agree not only near the stoichiometric regime, but also for the lean and rich mixtures (*MF*s). Close agreement over a wide range of *MF*s implies that heat losses were negligible in the experiment with hydrogen explosions. And, indeed, no soot was formed in this case and thus thermal losses from the transparent blue flame were minimal. On the other hand, in Fig. 5b – d, there is a close agreement only for the lean and stoichiometric *MF*s. For fuel-rich mixtures, the theoretical model tends to over-predict p_{max} because heat loss due to soot formation and radiation occurs in these experiments with hydrocarbons. Most of the soot is

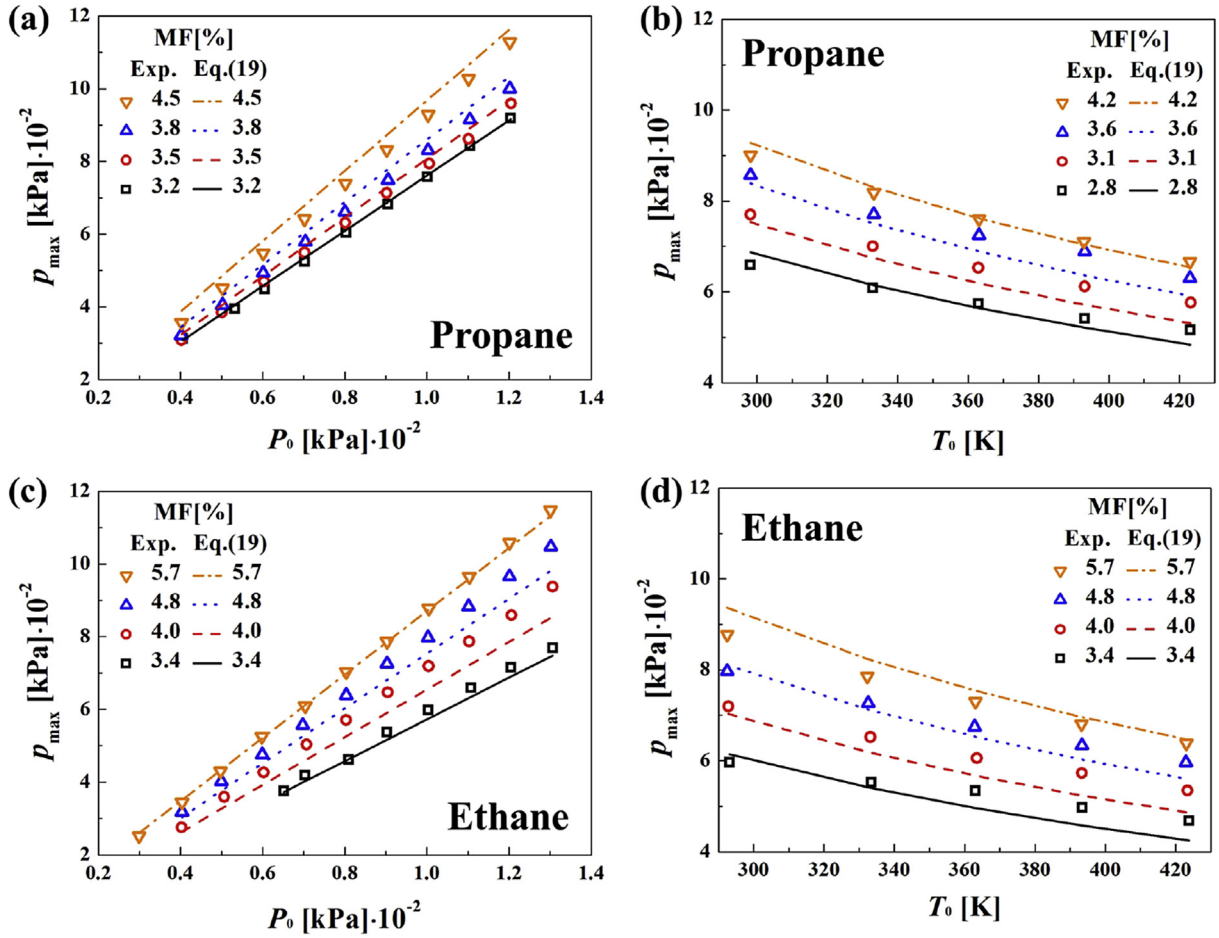

Fig. 7. Pressure p_{max} as a function of T_0 and p_0 for propane (a,b) and ethane (c,d). Experimental data for propane and ethane are from Refs. [4,5,20] and [4,5,20], respectively.

generated in rich mixtures, and also more soot is formed when more carbon is available. For example, there is more carbon in propane (C_3H_8) than in ethane (C_2H_6) or methane (CH_4); thus deviations between the theoretical predictions and experimental data increase from methane to propane.

Recall that $\eta_e = 1$ was used to calculate the theoretical curves in Fig. 5, which overestimates the amount of burned fuel-air mixture in partially closed confinements, especially in the rich mixtures for methane, ethane and propane. To account for the radiation heat loss due to soot formation for fuel-rich mixtures, η_e was adjusted so that the models matched the data. A linear dependence was used as $\eta_e = -a\,\mathrm{MF} + b$, where $a = 20$ and $b = 3.3$ for methane; $a = 35$ and $b = 4.5$ for propane; and $a = 24$ and $b = 3.5$ for ethane. The dashed curves in Fig. 5b – d shows an improved comparison between the experiments and the theoretical model with this adjustable η_e.

Sheroeder et al. [16] presented confined-space experimental data for p_{max} for different stoichiometric mixture temperatures of $T_0 = 293$, 373, 473, and 523 K for hydrogen at a fixed p_0. Within a confined space at p_0 being constant, the only way to vary T_0 was to extract a certain amount of the fuel-air mixture; otherwise, both T_0 and p_0 would increase because of confinement.

The pressure p_{max} at $T_0 = 293$ K is shown in Fig. 5 and not included in Fig. 6. The comparison for hydrogen, as mentioned above, revealed the best agreement between the theory of sub-section 2.1 and the experimental data because hydrogen combustion does not produce soot with the corresponding radiative heat losses (the case of $\eta_e = 1$). It should be emphasized that in Fig. 6 the theoretical predictions for different T_0 as correspond to different values of $\varepsilon = T_{bv}/T_0$, as per Eq. (20).

When T_0 increases, the value of p_{max} decreases. This is because the total number of the initial moles of mixture was decreased by removal of some of the fuel-air mixture from the confined space, as mentioned above. With less fuel, p_{max} decreases. From Eqs. (19) and (20), $\varepsilon = T_{bv}/T_0 = p_{max}/p_0$ when $\eta_e = 1$. If T_0 increases, ε decreases at a fixed adiabatic flame temperature ($\sim T_{bv}$) in a closed space, yielding a decreased p_{max} for fixed p_0 [17–19].

For a stoichiometric mixture, the heat release is maximized. The fact that heat losses happened, manifests itself in a slight over-prediction of p_{max} seen in Fig. 6 the stoichiometric cases. However, the overall good agreement of the theoretical predictions with the experimental data for hydrogen confirms that the effects of T_0 are accurately accounted for by the model.

Fig. 7 demonstrates the effects of p_0 and T_0 on p_{max} during explosion for $3.2\% \le MF \le 5.7\%$ (lean fuels). The experimental data for propane and ethane were adopted from Refs. [4,5,20]. The lean *MF* range was where the theory of **sub-section** and the experiment compared favorably, as mentioned above.

Fig. 7a and c shows that as p_0 increases from 0.4 to 1.2 bar (propane) and 1.3 bar (ethane), p_{max} also increases with a slope that increases with *MF*. More powerful explosions (greater p_{max}) are achieved when the fuel-air mixture approaches the stoichiometric ratio. For a given value of $\varepsilon = T_{bv}/T_0$, the relation between p_{max} and p_0 is linear according to Eqs. (19) and (20). This linear relation was validated by the experimental data. Fig. 7b and d shows that when

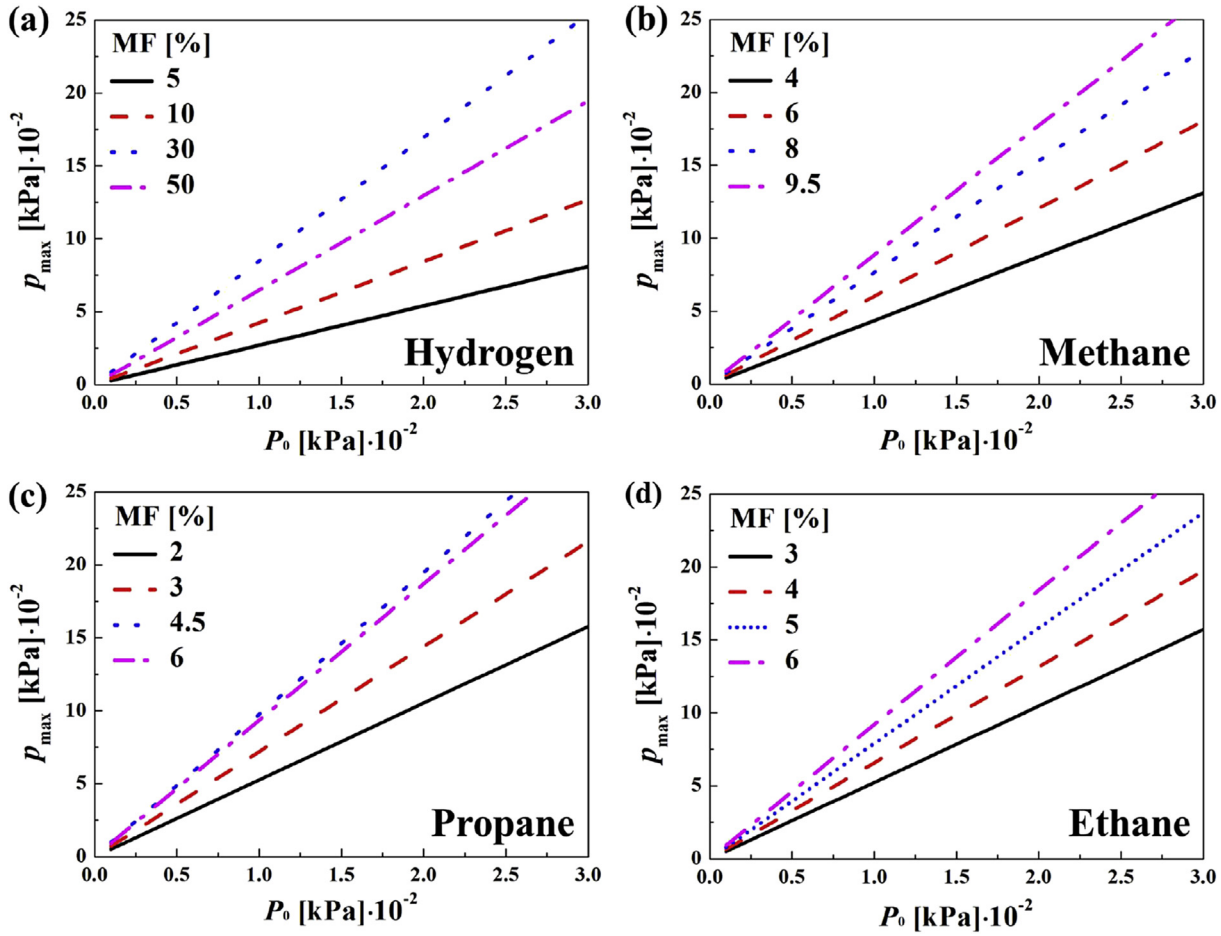

Fig. 8. Pressure p_{max} for varying initial pressure p_0 at a fixed $T_0 = 298$ K for hydrogen, (b) methane, (c) propane, (d) and ethane.

T_0 increases from 293 to 423 K for propane and ethane at a fixed p_0, p_{max} decreases for all values of *MF* because of the required reduction in fuel mass.

3.2. Parametric studies in the framework of the analytical thermodynamic model

Fig. 8 and 9 compare the effect of p_0 and T_0, respectively, on the maximum pressure p_{max} for varying *MF* of hydrogen, methane, propane, and ethane. The range of *MF* variation spans lean to stoichiometric ratios. Rich *MF* ratios were excluded because the theoretical model tends to over-predict p_{max} there. Figs. 8 and 9 are useful to field engineers to estimate p_{max} given the initial pressure and temperature p_0 and T_0 because it can be directly evaluated from these graphs without any numerical simulations.

For all cases, the highest value of p_{max} was observed at the stoichiometric *MF* ratios. In Fig. 8, p_{max} increases when the initial surrounding pressure, p_0, increases. In Fig. 9, $p_0 = 1$ bar, while T_0 changes from 300 to 500 K, which is a plausible temperature range at a petrochemical plant. Again, propane yields the highest p_{max}, followed by ethane, methane, and hydrogen, which corresponds to *MF*s of 4.5% for propane, 6% for ethane, 9.5% for methane, and 30% for hydrogen.

3.3. Numerical predictions by FLACS in comparison with the theoretical predictions of sub-section 3.1 and experimental data

Table 2 summarizes our two experiments used for comparison with theoretical and numerical predictions. Both experiments with propane (**Case 1–1 and 1–2**) and hydrogen (**Case 2**) were conducted for fuel-air mixtures near the stoichiometric ratios of 4.34–4.36% and 22.5%, respectively, resulting in the maximum pressures of $p_{max} = 43$ and 690 kPa for propane and hydrogen, respectively. As shown in Table 2, the same test was repeated twice (**Case 1–1** and **1–2**), which yielded the same p_{max} and nearly the same impulses and the effective duration. Therefore, the measurement was quite reliable with an uncertainty level of less than 8%.

Recall that these experiments were conducted in a congested space with an open wall at one-side (i.e., partially confined, and in the CFD calculations too), as described in Figs. 3 and 4, while a completely confined space was assumed in the theoretical model of sub-section 2.1 (Fig. 5).

Comparing the partially- and completely-confined scenarios offers an insight into two different combustion situations. For example, $p_{max} = 700$ kPa ($MF = 22.5\%$) predicted by the analytical model for the completely confined case in Fig. 5a, while the experimental measurement for the partially-confined space revealed $p_{max} = 690$ kPa. This minimal difference in these values of p_{max} implies that the combustion process between is nearly identical for hydrogen in these two cases. However, for propane, there is a significant difference in p_{max} between the completely and incompletely confined cases. From Fig. 5c, $p_{max} = 900$ kPa ($MF = 4.34\%$) for the completely confined space, while $p_{max} = 43$ kPa for the partially confined space. This difference is due to the lower burning velocity of propane that decreases the fuel-air

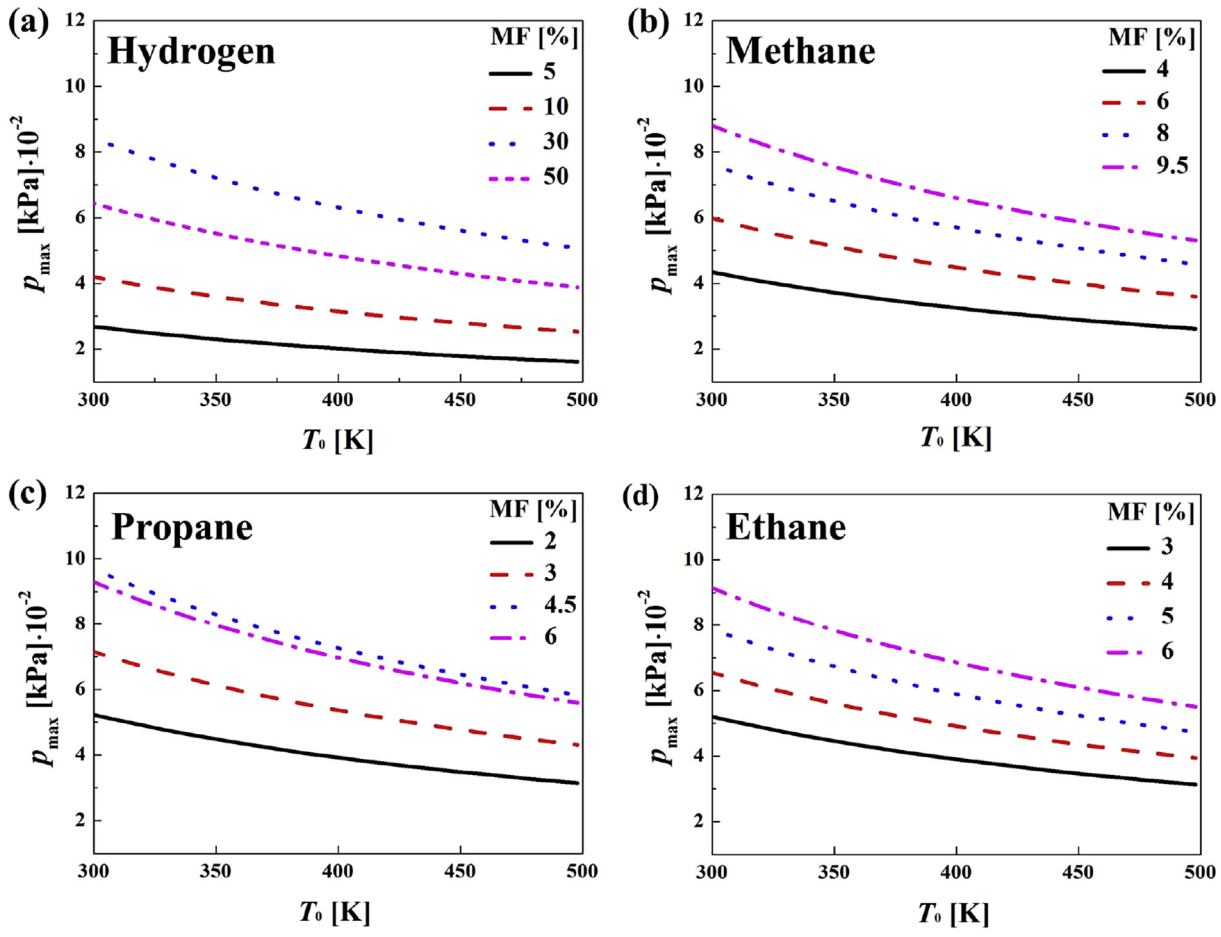

Fig. 9. Pressure p_{max} for varying initial temperature T_0 at a fixed $P_0 = 100$ kPa for (a) hydrogen, (b) methane, (c) propane, and (d) ethane.

Table 2
Peak values of p_{max} after ignition.

Case	Fuel	*MF* [%]	p_{max} [kPa]	Impulse [kPa-ms]	Effective duration [ms]
1–1	Propane (C_3H_8)	4.34	**43**	1448	73
1–2		4.36	**43**	1565	77
2	Hydrogen (H_2)	22.5	**690**	2850	10

Table 3
Experimental values for p_{max} compared to the theoretical analytical predictions from Eqs. (19) and (20) and the FLACS model.

Location			Experimental [kPa]		Theory [kPa]		CFD [kPa]	
			Case 1	Case 2	Case 1	Case 2	Case 1	Case 2
Interior	1	Rear	**43**	**690**	**89**	**727**	74	654
	2	Wall	**43**	680			**78**	**715**
	3	Column	40	**690**			51	707
	4	Floor	38	430			63	482
	5	Roof	34	470			64	487
Free-field	6	MP1	23	170	-		70	220
	7	MP2	19	140			58	175
	8	MP3	15	71			43	107
	9	MP4	11	47			30	77
	10	MP5	9.5	36			20	51
	11	MP6	7.7	28			14	38
	12	MP7	6.3	23			12	25

Table 4
Summary of grid-dependence studies.

Case	Fuel	p_{max} [kPa]				
		Experimental	Number of nodes [$\times 10^6$]			
			1 (low)	3.2 (med)	5 (hi)	7 (very hi)
1	Propane (C_3H_8)	43	65	72	**78**	79
2	Hydrogen (H_2)	690	310	658	**715**	718

mixing and slows down the chemical reaction in the partially confined space. In a completely confined space, p_{max} was as high as 900 kPa at $MF = 4.34\%$, both experimentally and theoretically (i.e. via the analytical model of sub-section 2.1) (see Fig. 5c), implying that the burning velocity of methane is practically as fast as that of hydrogen in a completely confined space.

Table 3 compares the values of p_{max} from the experiments, theoretical predictions, and the CFD model at various physical locations (i.e., rear wall, side walls, columns, floor, and roof as illustrated in Fig. 4). For methane **Case 1**, the theoretical prediction is $p_{max} = 89$ kPa assuming $\eta_e = 0.1$. In a completely confined space, $\eta_e = 1$, but this value is reduced here, since combustion takes place in a partially confined space. The corresponding CFD prediction for methane is $p_{max} = 78$ kPa, which also over-predicts the experimentally measured value of $p_{max} = 43$ kPa.

For hydrogen **Case 2**, the theoretical pressure is $p_{max} = 727$ kPa and from the CFD predictions it is $p_{max} = 715$ kPa, while for the experimental value is $p_{max} = 690$ kPa. These favorable comparisons indicate that the theoretical and numerical models are quite accurate in cases where a burning velocity is high and soot formation and the associated thermal losses are minimal.

Table 4 shows the grid-dependence studies carried out for computational discretizations ranging from 1 to 7 million nodes. Maximum pressures of $p_{max} = 78$ and 715 kPa for propane and hydrogen, respectively, showed convergence at about 5 million nodes. Thus, for all computations 5 million nodes were used.

Figs. 10 and **11** show snapshots from the explosions in the experiments and in the CFD simulations, respectively, for **Case 1** and **Case 2** as combustion progresses in time. The images for propane are up to 50 ms and those for hydrogen up to 20 ms. These results reveal that the almost stoichiometric hydrogen explosion is more powerful than that of propane. Fig. 12 compares p_{max} for these two cases (i.e., propane and hydrogen) as a function of the distance from the explosion apparatus. The location numbers from No. 1 to No. 5 correspond to the Rear Wall, Side Wall, Column, Floor, and Roof, as described in Fig. 4 while the physical locations corresponding to No. 6–12 are at $z = 11.9, 16.5, 22.6, 30.2, 37.8, 45.4$, and 53 m away from the open-end of the exploding container with an interval location of approximately 4–8 m between pressure gauges. At No. 12 (which is 53 m away from the container or ignition point), the pressure is assumed to be atmospheric.

4. Conclusion

A theoretical thermodynamic model for prediction of the maximum explosion pressure p_{max} was developed for lean, stoichiometric and rich fuel-air mixtures. The model was validated against the experimental data for hydrogen, methane, propane, and ethane explosions in a confined space. The effect of initial gas temperature and pressure on p_{max} was also studied. The

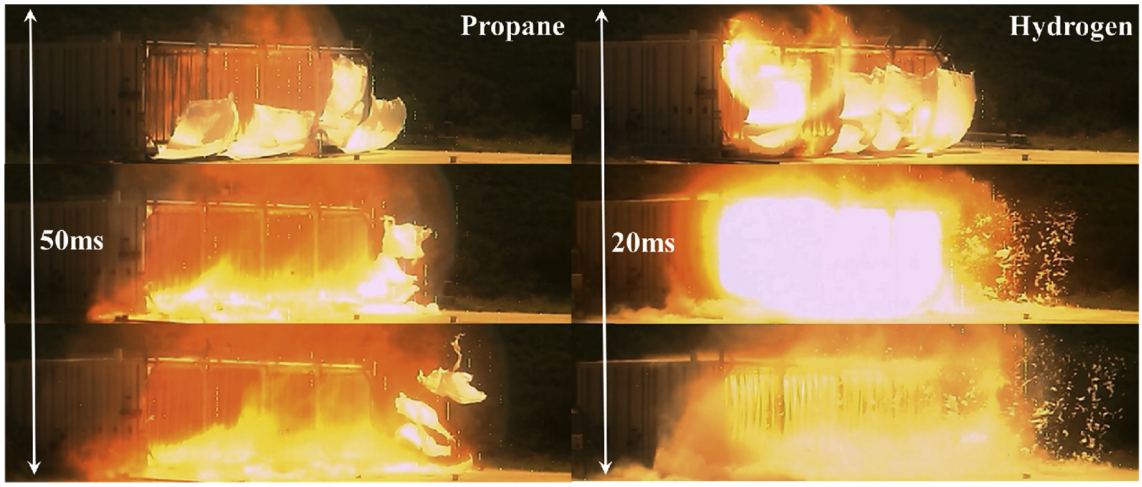

Fig. 10. Propane (Case 1) and hydrogen (Case 2) explosions observed by the high-speed camera.

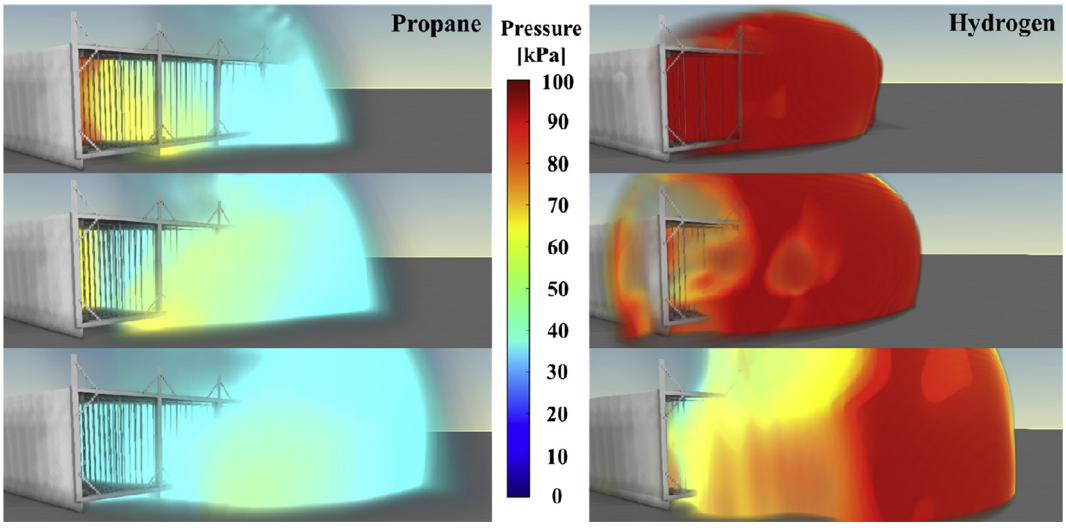

Fig. 11. Propane (Case 1) and hydrogen (Case 2) explosions from the numerical simulations.

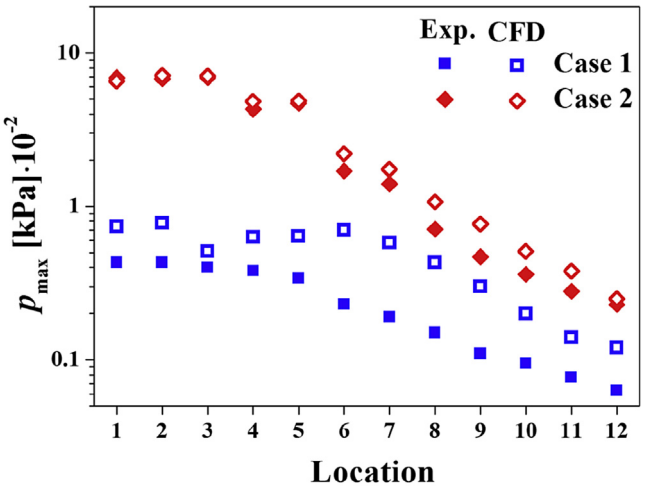

Fig. 12. Experimental and numerically predicted pmax as a function of distance. Note that No. 1–5 locations correspond to the interior pressure gauge locations, while No. 6–12 correspond to the exterior gauge-pressure locations, at z = 11.9, 16.5, 22.6, 30.2, 37.8, 45.4, and 53 m, respectively.

experimental data for propane and hydrogen deflagration in a partially confined space were acquired and also used to further validate the theoretical model, as well as the results of direct numerical simulations. For hydrogen at MF = 22.5%, the measured maximum pressure was p_{max} = 690 kPa, while that predicted by theory was 727 kPa. This close agreement indicates that the effects of a fully confined versus partially confined case are immaterial for rapidly exploding hydrogen. It also shows that soot formation and the associated radiative heat losses are negligible for hydrogen. Overall, the developed theoretical thermodynamic analytical model provides a conservative and accurate prediction for the maximum explosion pressure p_{max} for the methane-, ethane-, propane- and hydrogen-air mixtures at different values of the initial fuel mole fraction, pressure and temperature, MF, p_0 and T_0, respectively. The CFD model, FLACS, simulated congested experimental scenarios for propane and hydrogen explosions. The CFD model had a tendency to over-predict the pressure rise compared to experiments, but the differences remained within 10% and 5% for propane and hydrogen, respectively.

Acknowledgement

This research was primarily supported by Daewoo Institute of Construction and Technology. This work was also supported by the National Research Council of Science & Technology (NST) grant by the Korea government (MSIP) (No. CRC-16-02-KICT), NRF-2016M1A2A2936760, NRF-2017R1A2B4005639, and NRF-2013M3A6B1078879.

References

[1] Jo YD, Crowl DA. Flame growth model for confined gas explosion. Process Saf Prog 2009;28:141–6.
[2] Jo YD, Crowl DA. Explosion characteristics of hydrogen-air mixtures in a spherical vessel. Process Saf Prog 2010;29:216–23.
[3] Zhou B, Sobiesiak A, Quan P. Flame behavior and flame-induced flow in a closed rectangular duct with a 90 bend. Int J Therm Sci 2006;45:457–74.
[4] Razus D, Brinzea V, Mitu M, Oancea D. Temperature and pressure influence on explosion pressures of closed vessel propane–air deflagrations. J Hazard Mater 2010;174:548–55.
[5] Mitu M, Giurcan V, Razus D, Oancea D. Temperature and pressure influence on ethane–air deflagration parameters in a spherical closed vessel. Energy & Fuels 2012;26:4840–8.
[6] Bang B, Park H, Kim J, Al-Deyab SS, Yarin AL, Yoon SS. Analytical and numerical assessments of local overpressure from hydrogen gas explosions in petrochemical plants. Fire Mater 2016.
[7] Bang B, Park H-S, Kim J-H, Al-Deyab SS, Yarin AL, Yoon SS. Simplified method for estimating the effect of a hydrogen explosion on a nearby pipeline. J Loss Prev Process Ind. 2016;40:112–6.
[8] Luijten C, Doosje E, de Goey L. Accurate analytical models for fractional pressure rise in constant volume combustion. Int J Therm Sci 2009;48:1213–22.
[9] Zeldovich YB, Barenblatt GI, Librovich VB, Makhviladze GM. The Mathematical Theory of Combustion and Explosions. New York: Consultants Bureau, Plenum Press; 1985.
[10] Gexcon A. Flacs v10. 4r2 user's manual. Confidential report, Gexcon AS, Bergen, Norway. 2015.
[11] Launder BE, Spalding DB. The numerical computation of turbulent flows. Comput Methods Appl Mech Eng 1974;3:269–89.
[12] Patankar S. Numerical heat transfer and fluid flow. Boca Raton: CRC Press; 1980.
[13] Bray KNC. Studies of the turbulent burning velocity. Proc R Soc Lond A Math Phys Eng Sci R Soc 1990:315–35.
[14] Cashdollar KL, Zlochower IA, Green GM, Thomas RA, Hertzberg M. Flammability of methane, propane, and hydrogen gases. J Loss Prev Process Ind. 2000;13:327–40.
[15] Holtappels K., Liebner C., Schröder V., Schildberg H.-P., Report on experimentally determined explosion limits, explosion pressures and rates of explosion pressure rise-Part 2 Ethane, Ethylene, Propane, n-Butane, Ammonia and Carbon Monoxide, (2006).
[16] Schröder V., Holtappels K., Explosion characteristics of hydrogen-air and hydrogen-oxygen mixtures at elevated pressures, in: International

Conference on Hydrogen Safety, 2005.
[17] Gieras M, Klemens R, Rarata G, Wolański P. Determination of explosion parameters of methane-air mixtures in the chamber of 40dm 3 at normal and elevated temperature. J Loss Prev Process Ind. 2006;19:263–70.
[18] Huzayyin A, Moneib H, Shehatta M, Attia A. Laminar burning velocity and explosion index of LPG–air and propane–air mixtures. Fuel 2008;87:39–57.
[19] Razus D, Krause U. Comparison of empirical and semi-empirical calculation methods for venting of gas explosions. Fire Saf J 2001;36:1–23.
[20] Razus D, Movileanu C, Brinzea V, Oancea D. Explosion pressures of hydrocarbon–air mixtures in closed vessels. J Hazard Mater 2006;135:58–65.